Received: 1 November 2023 | Revised: 21 December 2023 | Accepted: 26 January 2024

DOI: 10.1002/mrm.30052

Magnetic Resonance in Medicine

TECHNICAL NOTE

High SNR full brain relaxometry at 7T by accelerated MR-STAT

Edwin Versteeg | **Hongyan Liu** | **Oscar van der Heide** | **Miha Fuderer** | **Cornelis A. T. van den Berg** | **Alessandro Sbrizzi**

Computational Imaging Group, Department of Radiotherapy, University Medical Center Utrecht, Utrecht, The Netherlands

Correspondence
Edwin Versteeg, Department of Radiology, University Medical Center Utrecht, Heidelberglaan 100, 3584CX Utrecht, the Netherlands.
Email: e.versteeg-5@umcutrecht.nl

Funding information
Nederlandse Organisatie voor Wetenschappelijk Onderzoek, Grant/Award Number: 18951

Abstract

Purpose: To demonstrate the feasibility and robustness of the Magnetic Resonance Spin TomogrAphy in Time-domain (MR-STAT) framework for fast, high SNR relaxometry at 7T.

Methods: To deploy MR-STAT on 7T-systems, we designed optimized flip-angles using the BLAKJac-framework that incorporates the SAR-constraints. Transmit RF-inhomogeneities were mitigated by including a measured B_1^+-map in the reconstruction. Experiments were performed on a gel-phantom and on five volunteers to explore the robustness of the sequence and its sensitivity to B_1^+ inhomogeneities. The SNR-gain at 7T was explored by comparing phantom and in vivo results to MR-STAT at 3T in terms of SNR-efficiency.

Results: The higher SNR at 7T enabled two-fold acceleration with respect to current 2D MR-STAT protocols at lower field strengths. The resulting scan had whole-brain coverage, with 1 x 1 x 3 mm^3 resolution (1.5 mm slice-gap) and was acquired within 3 min including the B_1^+-mapping. After B_1^+-correction, the estimated T_1 and T_2 in a phantom showed a mean relative error of, respectively, 1.7% and 4.4%. In vivo, the estimated T_1 and T_2 in gray and white matter corresponded to the range of values reported in literature with a variation over the subjects of 1.0%–2.1% (WM-GM) for T_1 and 4.3%–5.3% (WM-GM) for T_2. We measured a higher SNR-efficiency at 7T ($R = 2$) than at 3T for both T_1 and T_2 with, respectively, a 4.1 and 2.3 times increase in SNR-efficiency.

Conclusion: We presented an accelerated version of MR-STAT tailored to high field (7T) MRI using a low-SAR flip-angle train and showed high quality parameter maps with an increased SNR-efficiency compared to MR-STAT at 3T.

KEYWORDS

magnetic resonance imaging, quantitative imaging

1 | INTRODUCTION

Quantitative MRI techniques aim to directly estimate MR-specific tissue properties such as the relaxation rates T_1 and T_2, and the proton-density which can be used as biomarkers for disease progression in, for example, multiple sclerosis, brain tumors, and Parkinson' disease.[1–3] The main motivation for quantitative imaging at high field (≥7T) is the additional SNR available. This enables quantitative MRI techniques at higher resolutions and has been used to probe the brain's microstructure in terms of myelination, oxygenation, and iron content distribution.[4–8] In addition, the increased SNR can be used to obtain more precise and faster relaxometry than at lower field, where the available SNR is the main limitation on precision and scan time.[9–12]

Conventional quantitative MRI techniques are time-intensive as they estimate these tissue properties (T_1, T_2, proton-density) using multiple steady-state sequences with different sequence parameters to sensitize the sequence to a single parameter. Consequently, fast multi-parametric quantitative MRI techniques have been developed that simultaneously estimate multiple parameters from a single scan. Generally, these techniques use a transient-state sequence and a physics-based reconstruction and obtain the tissue parameters by either performing voxel-by-voxel dictionary matching on highly undersampled images (MR fingerprinting, or MRF)[9] or by directly solving for spatially resolved parameter maps from the time-domain signal (Magnetic Resonance Spin TomograPhy in Time-domain, or MR-STAT).[13]

The application of fast quantitative MR techniques at high field is challenging due to an increase in B_1^+-inhomogeneities and tissue heating (SAR), which both result from the higher RF frequencies used at 7T and beyond. Here, the B_1^+-inhomogeneities lead to spatially varying biases in the parameter maps which can be mitigated by including the B_1^+ as an extra parameter in the physics model. In such a model, the estimation of B_1^+ can be obtained by acquiring a separate B_1^+-map, by encoding the B_1^+ into the experiment by using a B_1^+-sensitive flip-angle train or by varying the RF-shims used during the experiment.[14–16]

An additional challenge for fast quantitative MR techniques is the high RF-power required. This originates from (i) the adiabatic inversion pulses used to improve T_1 encoding and reduce sensitivity to B_1^+, and (ii) the variable flip-angles which features large variations in flip-angle to ensure sufficient T_1 and T_2 encoding. The main approaches to limit SAR are a decrease in flip-angles or an increase in TR, which lead to a decrease in SNR of the estimated tissue parameters and longer scan times, respectively.

In this work, we demonstrate that the MR-STAT framework can be applied at high field (7T) by using a flip-angle train specifically optimized for 7T and by correcting for B_1^+-inhomogeneities using a short B_1^+-mapping scan and a TR-FOCI adiabatic inversion pulse.[17] In addition, we compare the SNR(−efficiency) of MR-STAT at 7T with the existing MR-STAT implementation at 3T and show that the additional SNR at 7T can be used to shorten the MR-STAT acquisition and obtain highly accurate mapping. This is demonstrated by applying two-fold undersampling, which leads to a full brain protocol with 1 x 1 x 3 mm^3 resolution (1.5 mm slice-gap) of 3 min. This protocol was validated in a gel phantom to test the accuracy and precision of the estimated T_1 and T_2 values and five healthy volunteers were scanned to demonstrate the feasibility and robustness.

2 | METHODS

MR-STAT enables the estimation of multi-parametric quantitative MR-maps directly from time-domain data of a single short scan. Here, the quantitative parameters are encoded into the signal by using a combination of Cartesian gradient encoding and a time-varying flip-angles during a non-balanced transient-state sequence. Quantitative parameter maps are obtained by directly and simultaneously solving for spatial localization and tissue parameters quantification in a single large-scale non-linear optimization process.[10,13]

2.1 | Sequence design

A typical unaccelerated MR-STAT acquisition repeats a linear phase-encoding pattern over a transient state flip-angle train where spin states are different for each phase encoding step. Spatial frequencies are sampled at the Nyquist rate and cover the equivalent of five or six full k-spaces (Figure 1). Acceleration can be achieved by skipping phase-encoding steps according to arbitrary design choices. Here, acceleration can be denoted by a factor R, similar to undersampling in conventional MR-acquisitions, which indicates the spatial frequencies omitted with respect to the unaccelerated (fully-sampled) MR-STAT sampling. The transient-state is achieved by using a series of varying RF-excitations which are preceded by an inversion pulse and are used to capture the time-domain signal needed to estimate T_1, T_2, and proton-density. To enable alias-free reconstruction when accelerating, we included receive coil sensitivities into the MR-STAT signal model, which enhance spatial encoding and can be obtained from a separate low-resolution scan. This leads to the following signal model:

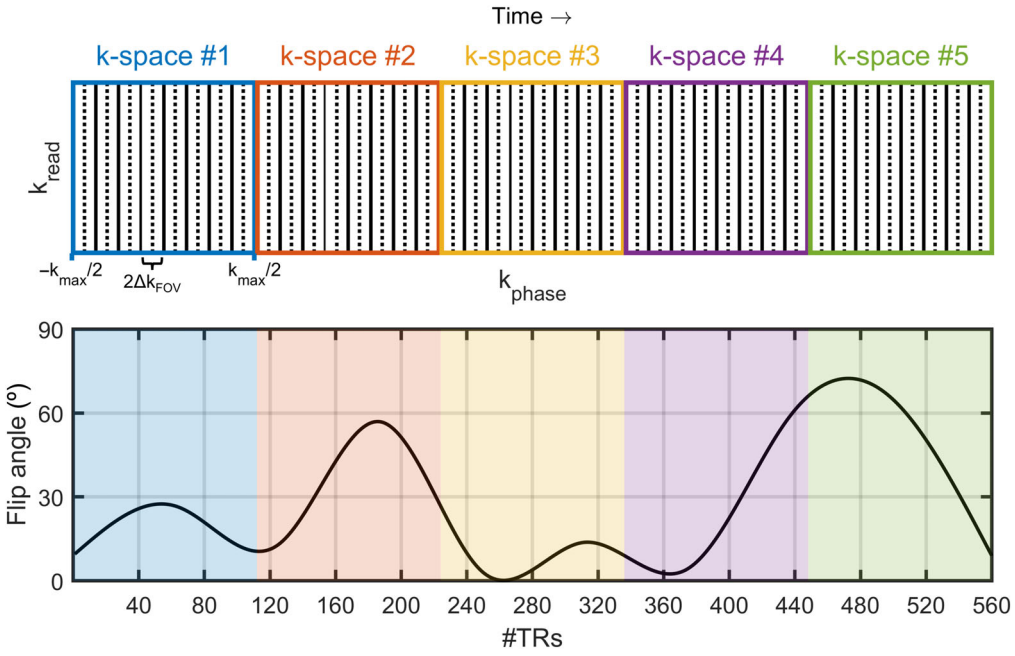

FIGURE 1 Top: A schematic depiction of the sampling scheme for the accelerated ($R = 2$) MR-STAT acquisition. Five k-spaces were acquired which were two-fold undersampled (indicated by the solid lines). Bottom: the BLAKJac-optimized low SAR flip-angle train.

$$S_n(t) = \int \rho(\boldsymbol{r}) C_n(\boldsymbol{r}) m(\boldsymbol{r}, \Theta(\boldsymbol{r}), t) d\boldsymbol{r} \quad (1)$$

where S_n is the temporal signal from each coil and ρ represents the proton-density that is spatially weighed by the receive sensitivity C_n of each receive coil. m denotes the spatial and temporal variation of the transverse magnetization during the MR-STAT experiments which depends on the spatial encoding and the applied RF-pulses, and MR-related parameters like T_1, T_2, and B_1^+ that are represented by Θ.

The BLAKJac[18] analytical framework was used to design a flip-angle train that minimizes the noise in the estimated T_1, T_2, and proton-density (ρ) while taking into account the phase-encoding pattern used alongside the varying flip-angles. The cost function used for the BLAKJac optimization contains a SAR penalty term based on the RMS flip-angle and TR which was used to optimize a flip-angle train specifically for low SAR by limiting the RMS flip-angle to 35° (excluding the inversion pulse). This value of 35° corresponded to the vendor defined low SAR condition for a TR of 11 ms. Furthermore, the optimization was performed for a set of eight T_1 and T_2 values which are typical for 7T brain imaging with T_1 ranging between 370 and 3300 ms and T_2 ranging between 25 and 308 ms. The resulting flip-angles and associated phase-encoding pattern can be found in Figure 1.

2.2 | Sequence parameters

Data were acquired in a gel-phantom and in vivo on a 7T MR-scanner (Philips, The Netherlands) using a 32-channel receive array (Nova Medical, USA) and a two-channel transmit coil (driven in quadrature). The imaging parameters were based on a previous clinical study performed with MR-STAT at 3T,[19] albeit with a longer TR/TE to limit SAR: voxel size = 1 x 1 mm^2, slice thickness = 3 mm, FOV = 224 x 224 mm^2, $N_{\text{slices}} = 5$ (gel-phantom) or 27 (in vivo), slice gap = 1.5 mm, TR = 11 ms and TE = 5.5 ms. Five Cartesian k-spaces were acquired for each slice to encode the quantitative parameters. For the two-fold undersampled scans (see Figure 1 for a schematic k-space sampling), this resulted in an acquisition time of 6 s per slice and 2′42″ s for the whole MR-STAT acquisition.

The B_1^+-inhomogeneities were estimated using a separate, 13 s long DREAM[20] sequence with a STEAM angle of 40 degrees, a 3.5 x 3.5 x 3.5 mm^3 isotropic resolution. The resulting B_1^+ map was subsequently used in the MR-STAT reconstruction. Receive coil sensitivity maps were obtained using ESPIRiT from the vendor's standard receive coil mapping scan.[21]

2.3 | Phantom experiments

Phantom experiments were performed on a phantom with 12 gel vials with varying T_1 and T_2 values (TO5, Eurospin II test system, Scotland). The effect of non-homogeneous B_1^+ on the MR-STAT reconstruction was tested by performing reconstructions with and without the measured B_1^+-prior. In addition, a two-fold undersampled acquisition was performed to investigate the effect of acceleration on the reconstructed parameters.

Ground truth values for T_1 and T_2 were obtained by acquiring a series of inversion recovery spin-echo acquisitions (T_1) and single-echo spin echo acquisitions (T_2) at varying inversion and TEs (10 TIs between 200 and 4150 ms and 10 TEs between 20 and 520 ms).

2.4 | In vivo experiments

Five volunteers (three male, two female, age 26–62) were scanned using the undersampled MR-STAT acquisition to assess the in vivo repeatability and enable comparison with relevant literature findings. Informed consent was given by all volunteers in accordance with the local Institutional Review Board for all scans. To enable comparison with literature values, a gray-white matter segmentation was performed using FSL (FAST)[22,23] on synthetic T_1-weighted images which were based on the R_1-maps ($1/T_1$).

2.5 | Comparison to 3T

In vivo and phantom data were also acquired on a 3T MR-scanner (Philips, The Netherlands) using a 15-channel receive array with identical imaging parameters except for a shorter TR and TE of 10.4 ms and 5.2 ms, respectively. A flip-angle train specifically optimized for 3T was used which also featured a flip-angle constraint of 35 degrees rms. Due to SNR-constraints, the in vivo data at 3T were acquired without undersampling while the phantom data were acquired both fully sampled ($R=1$) and two-fold undersampled ($R=2$). B_1^+ and coil sensitivity maps were acquired similarly to the data at 7T to allow for B_1^+-correction during the reconstruction.

The phantom data from 7T and 3T were used to calculate SNR-efficiency for T_1 and T_2 using[9]:

$$\mathrm{SNR}_{\mathrm{efficiency},T_n} = \frac{T_n\mathrm{NR}}{\sqrt{T_{\mathrm{scan}}}}, \quad \text{with} \quad n = 1, 2. \tag{2}$$

Here, T_nNR is the SNR for T_1 or T_2 based on the mean of the T_1/T_2 divided by the SD over each vial. T_{scan} is the scan time per slice in seconds.

2.6 | Reconstruction

The MR-STAT reconstructions were performed on a GPU (NVIDIA, A5000) using a reconstruction algorithm written in the Julia programming language.[24] This reconstruction algorithm included an EPG-simulator to compute the forward signal model and the partial derivatives with respect to the tissue parameters for the spoiled gradient sequence. For this work, the EPG simulator was adapted to include the history of inversion pulses applied to each slice before acquiring the data, an explanation on the necessity of this adaption is found in the supplementary information (Figure S1).

The reconstruction also included slice-profile effects which were included by using Bloch equation simulations for 35 sub-slices equally distributed along the slice-selection direction over a range of three times the nominal slice-thickness.[25]

3 | RESULTS

3.1 | Phantom experiments

Figure 2A shows a comparison between the reconstructed T_1 and T_2 values per vial without and with B_1^+-correction for the fully-sampled and accelerated MR-STAT acquisitions. Here, the effect of the B_1^+-correction was similar for both acquisitions. Specifically, the reconstructed T_1 values did not significantly change after correcting for B_1^+ with a mean relative error of 2.9% ($R=1$) and 1.7% ($R=2$) with respect to the ground truth values. The reconstructed T_2 values, on the other hand, did change significantly when correcting for B_1^+ as this caused the mean relative error to decrease from 33.5% ($R=1$) and 30.2% ($R=2$) to 4.2% ($R=1$) and 4.4% ($R=2$). After B_1^+-correction, both fully-sampled and undersampled data yielded similar T_1 and T_2 estimates with a mean relative difference of 1.6% for T_1 and 2.4% for T_2.

Figure 2B shows the effect of the B_1^+-inhomogeneities on the reconstructed T_1, T_2, and proton-density for the gel phantom for $R=2$. Here, the inclusion of the B_1^+-map in the reconstruction mainly affected the T_2 and proton-density reconstructions (Figure 2B). The artifact highlighted by the red arrows was caused by a large B_0-inhomogeneity (~400 Hz) at an air-water boundary, which could not be mitigated by B_0-shimming. As such, these vials were omitted from the quantitative plots in Figure 2A.

3.2 | In vivo experiments

Figure 3(A,B) shows two representative slices for two subjects at 7T (the rest of the slices and subjects can be found in Figure S2 of the supporting information). All parameter maps show a low noise level allowing for a clear distinction between gray and white matter and smaller structures like the basal ganglia (Figure 3A). Figure 3B shows a slice lower in the brain where a bias in T_2 and T_1 values was observed

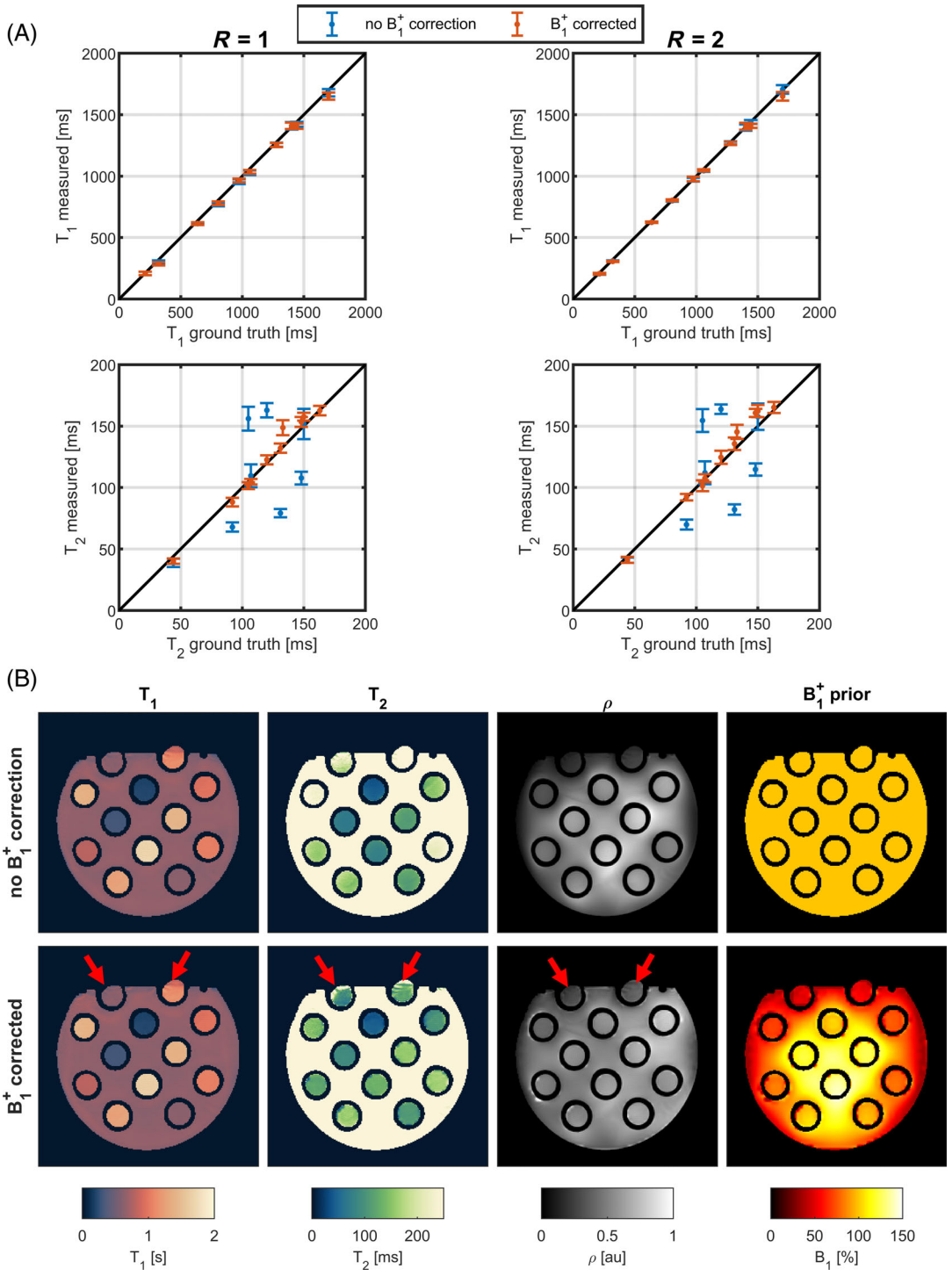

FIGURE 2 Results for the phantom experiments at 7T. (A) comparison of the reconstructed quantitative values with ($R = 2$) and without ($R = 1$) acceleration and with (red) and without (blue) B_1^+-correction. (B) The reconstructed T_1, T_2, and proton-density maps for the accelerated MR-STAT acquisition ($R = 2$) showing the effect of including a measured B_1^+-map in the reconstruction. Here, the red arrows highlight vials that display an artifact originating from a large B_0-inhomogeneity.

in the cerebellum due to a combination of a bias in the B_1^+ mapping at extremely low B_1^+ (<20% of the nominal B_1^+, indicated by the green arrows in Figure 3B) and B_0 inhomogeneities (yellow arrows in Figure 3B) close to the ear cavities resulting in imperfect inversion. In addition, we observed minor pulsatility artifacts in the phase-encoding direction originating from blood flow in large vessels (red arrows in Figure 3A).

Figure 3C shows the distribution T_1 and T_2 values in the gray and white matter over the whole-brain across all

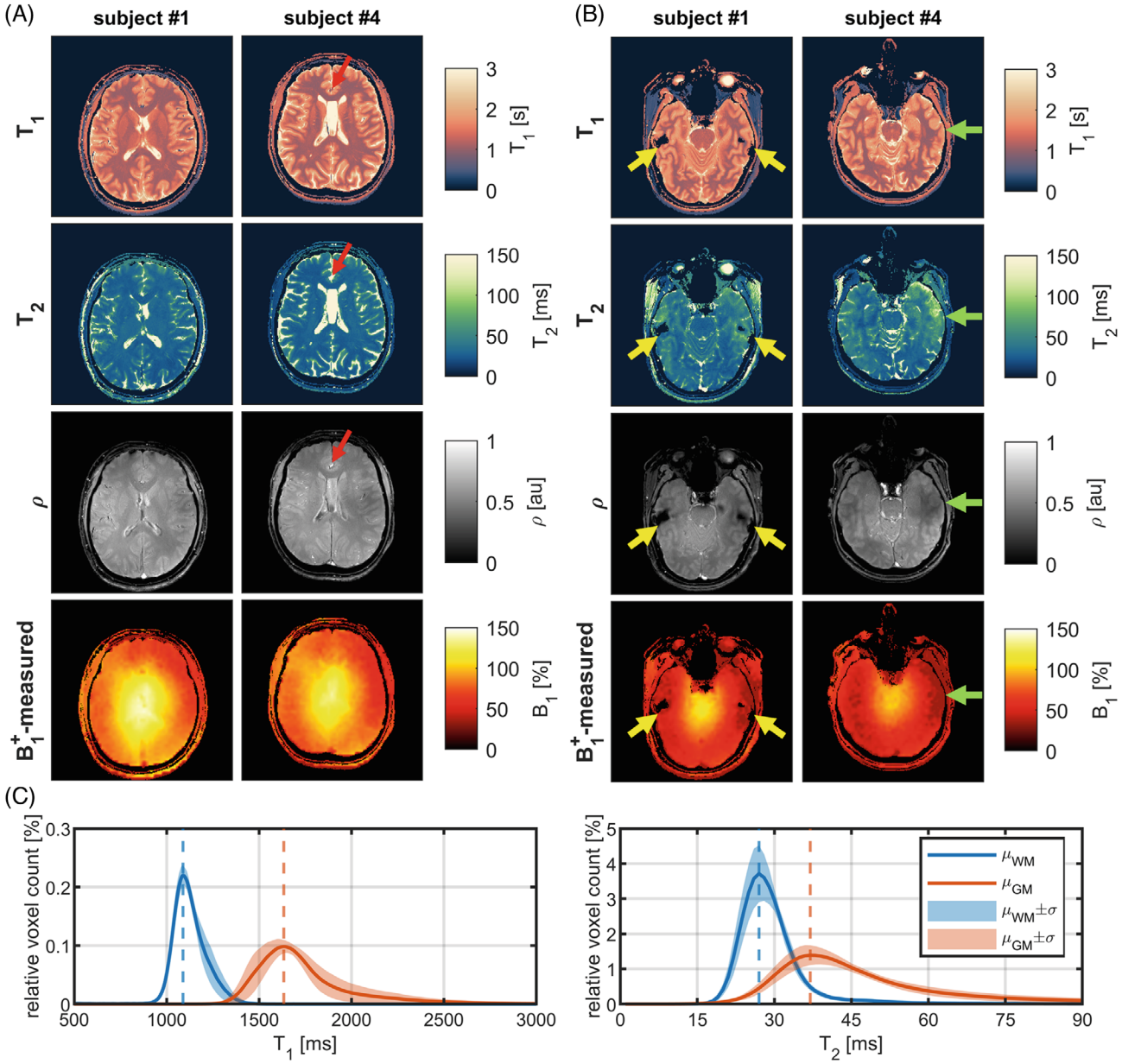

FIGURE 3 Reconstructed T_1, T_2, and proton-density (ρ) and the measured B_1^+-map used during reconstruction for two representative slices in two subjects. (A) A central slice with relatively homogeneous B_1^+. Here, the red arrow highlights an artifact originating from blood pulsation. (B) A slice in the lower brain with inhomogeneous B_1^+ and B_0. Here, the yellow arrows point toward susceptibility artifacts caused by B_0-inhomogeneities around the ears. The green arrows highlight a bias in T_2 values which is observed in areas of low B_1^+ (<35% of the nominal B_1^+). (C) The distribution of T_1 and T_2 values in gray and white matter across the five volunteers.

subjects. The peak values for the reconstructed T_1 and T_2 are summarized in Table 1. Here, the reconstructed T_1 was found to be 1092 ± 11 ms (1.0% inter-subject variation) in white matter and 1610 ± 34 ms (2.1% inter-subject variation) in the gray matter. The reconstructed T_2 varied from 28 ± 1.2 ms (4.3% inter-subject variation) in the white matter to 36 ± 1.9 ms (5.3% inter-subject variation) in the gray matter. Both the observed T_1 and T_2 values fall in the range of values reported previously in the relevant literature (Table 1).[26–30]

3.3 | Comparison to 3T

Figure 4A,B shows the SNR(−efficiency) for unaccelerated and accelerated MR-STAT acquisitions on a phantom at 3T and 7T. Figure 4A shows that the SNR at 7T is consistently higher than at 3T for an RMS flip-angle of 35 degree. In the Figure S4, this is shown to also hold when an RMS flip-angle of 70 degrees is used at 3T. Additionally, the SNR in T_1 at 7T was observed to not decrease for two-fold undersampling. Overall, a higher SNR-efficiency

TABLE 1 Reconstructed T_1 and T_2 values for the different subjects.

	Reconstructed T_1 [ms]		Reconstructed T_2 [ms]	
Subject	**WM**	**GM**	**WM**	**GM**
1	1106	1611	28	34
2	1082	1565	28	36
3	1086	1600	27	35
4	1084	1620	27	36
5	1102	1658	30	39
$\mu \pm \sigma$	1092 ± 11	1610 ± 34	28 ± 1.2	36 ± 1.9
Literature (min–max)	924–1394	1451–2000	25–39	33–55

Note: The values were obtained from the peak of the gray and white matter histograms. On the bottom the range of literature values for T_1 and T_2.

was observed for the MR-STAT acquisitions at 7T with a 3.1 ($R = 1$) and 4.1 ($R = 2$) times increase in SNR-efficiency for T_1 and a 2.2 ($R = 1$) and 2.3 times ($R = 2$) increase for T_2. Importantly, the SNR-efficiency remained relatively constant for unaccelerated and accelerated acquisitions at 3T while an increased SNR-efficiency in T_1 was observed for the accelerated scan at 7T.

The in vivo 3T and 7T results in Figure 4C also highlight the increased SNR at 7T which can primarily be seen in the T_2 and proton-density maps.

4 | DISCUSSION AND CONCLUSIONS

In this work, we demonstrated an accelerated MR-STAT acquisition at 7T that yielded high-quality quantitative parameters maps both in-vitro and for full-brain in five healthy volunteers. This was enabled by a flip-angle train that was optimized for low SAR, and for the expected T_1 and T_2 values occurring at 7T using the BLAKJac framework. In addition, we showed an increase in SNR-efficiency compared to MR-STAT at 3T and a reduction in the sensitivity to B_1^+ variations by incorporating measured B_1^+-maps.

The phantom experiments highlighted the necessity of B_1^+-correction especially for estimation of the T_2. Specifically, the variations in B_1^+ at 7T (between 50% and 150% of the nominal B_1^+) caused a mean relative error of 30.2% in the reconstructed T_2 if not taken into account. After B_1^+-correction, this error was reduced to 4.4% ($R = 2$) which was primarily caused by a bias (overestimation) at higher (>100 ms) T_2 values. In addition to imperfect B_1^+, the B_0 fluctuation was also found to influence the reconstructed T_1 and T_2 values, which was caused by aliasing of signals with a larger difference in B_0 offset (>100 Hz).

In vivo, we observed residual influences of B_1^+-inhomogeneities in the cerebellum on the reconstructed parameters. Here, an underestimation of T_1 value was still observed in areas of extremely low B_1^+ (<20% of the nominal B_1^+) where the adiabatic condition for the inversion pulse was not met. Notably, these areas of low B_1^+ also featured a bias in T_2 values due to a lack of T_2 encoding, which was caused by the low effective flip-angle reached in these areas. To improve B_1^+-coverage, a multi-transmit RF-coil could be used to provide a more homogeneous B_1^+ (RF shimming) and more importantly to achieve high B_1^+ over a larger volume.[31,32]

At 7T, similar T_1 and T_2 values were found across the five human subjects with a SD between 1% and 2% (WM-GM) for T_1 and 5%–6% (WM-GM) for T_2 and fit within the range of values reported previously in literature. Here, the largest variability between subjects possibly originated from variations in head sizes affecting the coil loading, which resulted in different B_1^+-profiles and slightly different RF-power used for scans. In literature, the RF-power has been identified as one of the main confounders for variability in quantitative parameter mapping,[33–36] as changes in RF-power will exacerbate magnetization transfer effects and change the effectively measured T_1 and T_2. These effects could potentially be incorporated into the MR-STAT signal model albeit at the cost of extra computational complexity and scan time.

The accuracy of the B_1^+-map is the main limitation of the approach presented in this work. Especially at very low B_1^+ (<30%), the accuracy of the DREAM sequence is limited leading to a bias in T_2 values in the cerebellum. This could be improved by using a multi-transmit setup with larger B_1^+-coverage. Alternatively, direct estimation of the B_1^+ could also be considered with the MR-STAT framework by using a B_1^+-sensitive flip-angle train.[14,15,37] However, this could potentially increase scan time as more time might be needed to ensure sufficient encoding of B_1^+ along with T_1 and T_2.

Compared to MR-STAT at 3T, the phantom results showed an expected increase in SNR-efficiency when going to 7T for both T_1 and T_2. In addition, an increase in SNR-efficiency for T_1 was observed when accelerating MR-STAT at 7T. The in vivo accelerated parameter maps at 7T showed a higher SNR when compared to fully-sampled MR-STAT at 3T. Given these results, we hypothesize that further increases in SNR-efficiency could be achieved by combining MR-STAT with a simultaneous multi-slice (SMS) approach[38–40] or by extending MR-STAT to 3D to yield a higher through-plane resolution while allowing for higher acceleration factors.[41]

In conclusion, we presented an extension of the MR-STAT to high field (7T) and showed that whole-brain

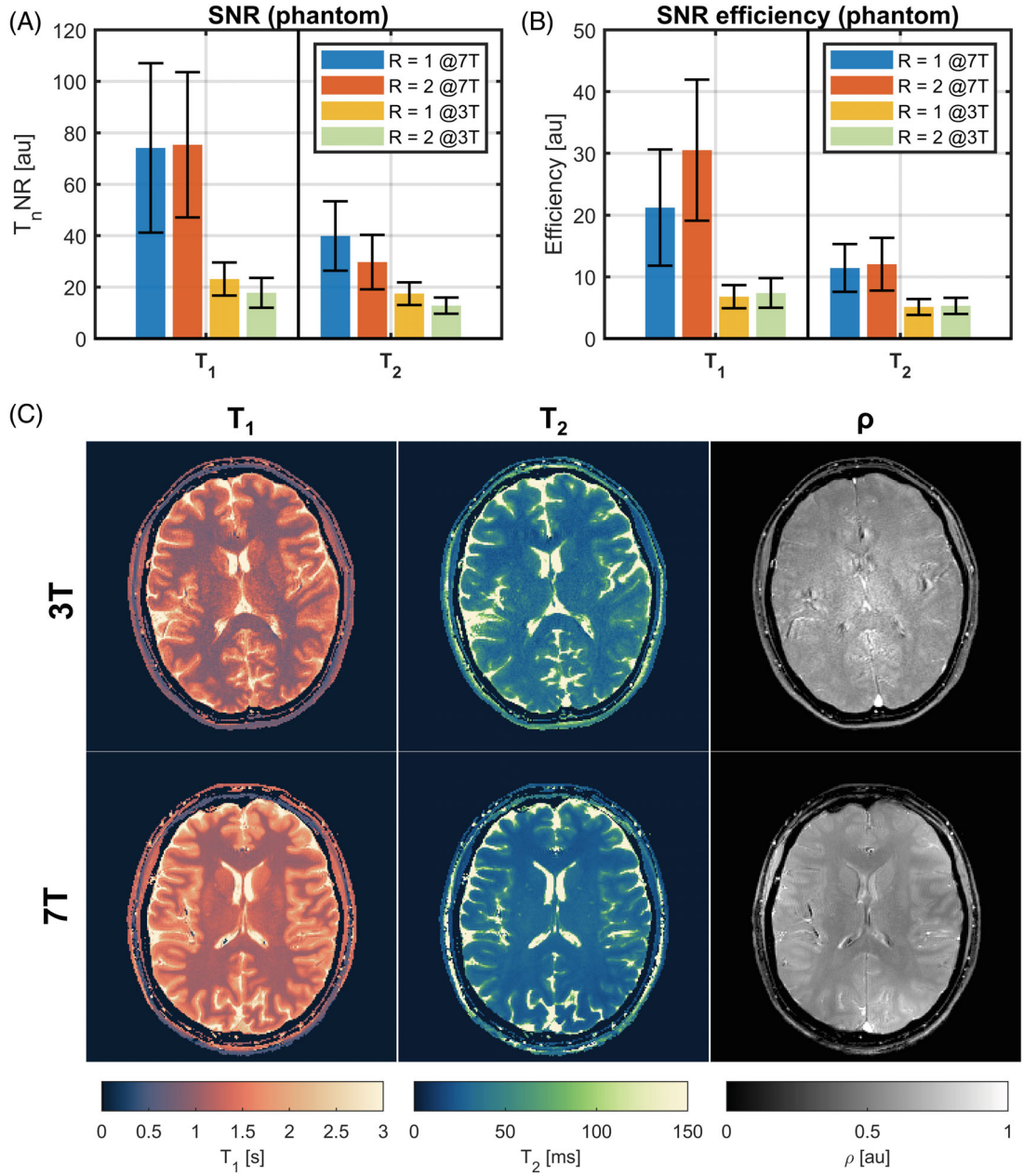

FIGURE 4 Results for the comparison between MR-STAT at 3T vs 7T. The measured SNR (A) and SNR-efficiency (B) for T_1 and T_2 in phantom experiments which show higher SNR(−efficiency) at 7T for both $R = 1$ and $R = 2$. (C) In vivo MR-STAT reconstructions at 3T ($R = 1$) and 7T ($R = 2$) which show the increased SNR when going to 7T. The other slices of the volumes can be found in Figure S3 of the supporting information.

coverage is possible within 3 min. The resulting quantitative parameter maps showed a low noise level and should therefore be suitable for studying disease progression and microstructure in the brain at 7T.

ACKNOWLEDGMENTS

This work has been financed by NWO grant number 18951.

ORCID

Edwin Versteeg https://orcid.org/0000-0003-3235-3970
Hongyan Liu https://orcid.org/0000-0002-1319-0419
Oscar van der Heide https://orcid.org/0000-0002-8451-525X
Miha Fuderer https://orcid.org/0000-0002-5673-915X

REFERENCES

1. Cercignani M, Dowell N, Tofts P. Quantitative MRI of the Brain: Principles of Physical Measurement. Quantitative MRI of the Brain: Principles of Physical Measurement; 2018.
2. Lescher S, Jurcoane A, Veit A, Bähr O, Deichmann R, Hattingen E. Quantitative T_1 and T_2 mapping in recurrent

glioblastomas under bevacizumab: earlier detection of tumor progression compared to conventional MRI. *Neuroradiology*. 2015;57:11-20.
3. Vymazal J, Righini A, Brooks RA, et al. T_1 and T_2 in the brain of healthy subjects, patients with Parkinson disease, and patients with multiple system atrophy: relation to iron content. *Radiology*. 1999;211:489-495.
4. Callaghan MF, Helms G, Lutti A, Mohammadi S, Weiskopf N. A general linear relaxometry model of R1 using imaging data. *Magn Reson Med*. 2015;73:1309-1314.
5. Bhogal AA, Siero JCW, Zwanenburg J, Luijten PR, Philippens MEP, Hoogduin H. Quantitative T_1 mapping under precisely controlled graded hyperoxia at 7T. *J Cereb Blood Flow Metab*. 2017;37:1461-1469.
6. Waehnert MD, Dinse J, Schäfer A, et al. A subject-specific framework for in vivo myeloarchitectonic analysis using high resolution quantitative MRI. *Neuroimage*. 2016;125:94-107.
7. Fritz FJ, Poser BA, Roebroeck A. MESMERISED: super-accelerating T1 relaxometry and diffusion MRI with STEAM at 7 T for quantitative multi-contrast and diffusion imaging. *Neuroimage*. 2021;239:118285.
8. Caan MWA, Bazin PL, Marques JP, de Hollander G, Dumoulin SO, van der Zwaag W. MP2RAGEME: T1, T_2^*, and QSM mapping in one sequence at 7 tesla. *Hum Brain Mapp*. 2019;40:1786-1798.
9. Ma D, Gulani V, Seiberlich N, et al. Magnetic resonance fingerprinting. *Nature*. 2013;495:187-192.
10. van der Heide O, Sbrizzi A, Luijten PR, van den Berg CAT. High-resolution in vivo MR-STAT using a matrix-free and parallelized reconstruction algorithm. *NMR Biomed*. 2020;33:1-16.
11. van der Heide O, Sbrizzi A, van den Berg CAT. Cartesian vs radial MR-STAT: an efficiency and robustness study. *Magn Reson Imaging*. 2023;99:7-19.
12. Assländer J. A perspective on MR fingerprinting. *J Magn Reson Imaging*. 2021;53:676-685.
13. Sbrizzi A, van der Heide O, Cloos M, et al. Fast quantitative MRI as a nonlinear tomography problem. *Magn Reson Imaging*. 2018;46:56-63.
14. Buonincontri G, Sawiak SJ. MR fingerprinting with simultaneous B_1 estimation. *Magn Reson Med*. 2016;76:1127-1135.
15. Buonincontri G, Schulte RF, Cosottini M, Tosetti M. Spiral MR fingerprinting at 7 T with simultaneous B_1 estimation. *Magn Reson Imaging*. 2017;41:1-6.
16. Cloos MA, Knoll F, Zhao T, et al. Multiparametric imaging with heterogeneous radiofrequency fields. *Nat Commun*. 2016;7:7.
17. Hurley AC, Al-Radaideh A, Bai L, et al. Tailored RF pulse for magnetization inversion at ultrahigh field. *Magn Reson Med*. 2010;63:51-58.
18. Fuderer M, van der Heide O, Liu H, van den Berg CAT, Sbrizzi A. Efficient performance analysis and optimization of transient-state sequences for multi-parametric MRI. *NMR Biomed*. 2022;36:e4864.
19. Kleinloog JPD, Mandija S, D'Agata F, et al. Synthetic MRI with magnetic resonance spin TomograPhy in time-domain (MR-STAT): results from a prospective cross-sectional clinical trial. *J Magn Reson Imaging*. 2022;57:1451-1461.
20. Nehrke K, Börnert P. DREAM-a novel approach for robust, ultrafast, multislice B_1 mapping. *Magn Reson Med*. 2012;68:1517-1526.
21. Uecker M, Lai P, Murphy MJ, et al. ESPIRiT-an eigenvalue approach to autocalibrating parallel MRI: where SENSE meets GRAPPA. *Magn Reson Med*. 2014;71:990-1001.
22. Jenkinson M, Beckmann CF, Behrens TEJ, Woolrich MW, Smith SM. Fsl. *NeuroImage*. 2012;62:782-790.
23. Zhang Y, Brady M, Smith S. Segmentation of brain MR images through a hidden Markov random field model and the expectation-maximization algorithm. *IEEE Trans Med Imaging*. 2001;20:45-57.
24. van der Heide O, Sbrizzi A, van den Berg CAT. Faster Bloch simulations and MR-STAT reconstructions on GPU using the Julia programming language. In: Proceedings of the 30th Annual Meeting of ISMRM; 2021. p. 3063.
25. Pauly J, Nishimura D, Macovski A, Le RP. Parameter relations for the Shinnar-Le roux selective excitation pulse design algorithm. *IEEE Trans Med Imaging*. 1991;10:53-65.
26. Marques JP, Kober T, Krueger G, van der Zwaag W, Van de Moortele PF, Gruetter R. MP2RAGE, a self bias-field corrected sequence for improved segmentation and T_1-mapping at high field. *Neuroimage*. 2010;49:1271-1281.
27. Emmerich J, Flassbeck S, Schmidt S, Bachert P, Ladd ME, Straub S. Rapid and accurate dictionary-based T_2 mapping from multi-echo turbo spin echo data at 7 tesla. *J Magn Reson Imaging*. 2019;49:1253-1262.
28. Yu Z, Madelin G, Sodickson DK, Cloos MA. Simultaneous proton magnetic resonance fingerprinting and sodium MRI. *Magn Reson Med*. 2020;83:2232-2242.
29. Yu Z, Hodono S, Dergachyova O, et al. Simultaneous 3D acquisition of 1H MRF and 23Na MRI. *Magn Reson Med*. 2022;87:2299-2312.
30. Olsson H, Andersen M, Kadhim M, Helms G. MP3RAGE: simultaneous mapping of T_1 and B_1^+ in human brain at 7T. *Magn Reson Med*. 2022;87:2637-2649.
31. Katscher U, Börnert P, Leussler C, Van den Brink JS. Transmit SENSE. *Magn Reson Med*. 2003;49:144-150.
32. Zhu Y. Parallel excitation with an array of transmit coils. *Magn Reson Med*. 2004;51:775-784.
33. Malik SJ, Teixeira RPAG, Hajnal JV. Extended phase graph formalism for systems with magnetization transfer and exchange. *Magn Reson Med*. 2018;80:767-779.
34. Rui RP, Malik SJ, Hajnal JV. Fast quantitative MRI using controlled saturation magnetization transfer. *Magn Reson Med*. 2019;81:907-920.
35. Rioux JA, Levesque IR, Rutt BK. Biexponential longitudinal relaxation in white matter: characterization and impact on T_1 mapping with IR-FSE and MP2RAGE. *Magn Reson Med*. 2016;75:2265-2277.
36. Hilbert T, Xia D, Block KT, et al. Magnetization transfer in magnetic resonance fingerprinting. *Magn Reson Med*. 2020;84:128-141.
37. Körzdörfer G, Jiang Y, Speier P, et al. Magnetic resonance field fingerprinting. *Magn Reson Med*. 2019;81:2347-2359.
38. Larkman DJ, Hajnal JV, Herlihy AH, Coutts GA, Young IR, Sta EG. Use of multicoil arrays for separation of signal from multiple slices simultaneously excited. *J Magn Reson Imaging*. 2001;13:313-317.
39. Ye H, Ma D, Jiang Y, et al. Accelerating magnetic resonance fingerprinting (MRF) using t-blipped simultaneous multislice (SMS) acquisition. *Magn Reson Med*. 2016;75:2078-2085.

40. Ye H, Cauley SF, Gagoski B, et al. Simultaneous multislice magnetic resonance fingerprinting (SMS-MRF) with direct-spiral slice-GRAPPA (ds-SG) reconstruction. *Magn Reson Med*. 2017;77:1966-1974.
41. Liu H, van der Heide O, Fuderer M, Berg CAT, Van Den SA. 3D MR-STAT: towards a fast multi-parametric protocol with increased SNR. In: Proceedings of the 31st Annual Meeting of ISMRM; 2022. p. 1348.

SUPPORTING INFORMATION

Additional supporting information may be found in the online version of the article at the publisher's website.

Figure S1. (A) The simulated effect of the inversion pulse on the signal evolution of white matter ($T_1/T_2 = 1090/29$ ms), gray matter ($T_1/T_2 = 1700/40$ ms) and CSF ($T_1/T_2 = 3000/200$ ms) when using the single inversion pulse model and the multi inversion pulse model. The time between slices was ∼6.2 s which is the same as was used in all the measurements in this work. Note here that the largest deviation in signal evolution is observed for tissues with a long >1500 ms T_1. (B) the effect of the multi inversion pulse model on in vivo data for a slice to which already six inversion pulses have been applied. The largest effect is seen in the CSF where the reconstructed T_1 is increased by at least 500 ms, while a smaller effect is seen in gray matter with T_1 values increasing between 50 and 100 ms.

Figure S2. Complete volumes for all subjects based on Figure 3 showing the reconstructed T_1, T_2 and proton-density (ρ) and the measured B_1^+ − map used during reconstruction.

Figure S3. Complete volumes for all subjects based on Figure 4 showing the in vivo MR-STAT reconstructions at 3 T($R = 1$) and 7 T ($R = 2$) which show the increased SNR when going to 7 T.

Figure S4. Results for the comparison between MR-STAT at 3T vs 7T. The measured SNR (Left) and SNR-efficiency (Right) for T_1 and T_2 in phantom experiments which show higher SNR(-efficiency) at 7T for both $R = 1$ and $R = 2$. Here, we also see that allowing a higher root-mean-square flip-angle at 3T of 70 degrees only results in a small ∼20% increase in the SNR in T_1/T_2.

How to cite this article: Versteeg E, Liu H, van der Heide O, Fuderer M, van den Berg CAT, Sbrizzi A. High SNR full brain relaxometry at 7T by accelerated MR-STAT. *Magn Reson Med*. 2024;92:226-235. doi: 10.1002/mrm.30052